Journal of Forestry Research and Management. Vol. 19(4).18-30; 2022, ISSN 0189-8418

www.jfrm.org.ng

Tasselled Cap Indices and Thermal Interactions in a Forest Ecosystem, a Geospatial Approach.

*Aigbokhan O. J., Pelemo O. J., Afolabi O. S., Essien N. E., Mba N. C.

Department of Environmental Modeling and Biometrics.
Forestry Research Institute of Nigeria, Jericho Hill, Ibadan.
Corresponding Author's email: oseyomon255@gmail.com.

ABSTRACT

An important result of anthropogenic activities inside and outside of a forest ecosystem is the destruction of vegetation. These changes can easily be seen and estimated with aid of satellite imagery, remote sensing and geographic information system (GIS) technology. Tasselled cap indices offer a more thorough representation of many geographical features, including vegetation, water, and bare terrain. The Landsat multi-spectral scanner (MSS) has undergone considerable upscales to work with contemporary sensors. Landsat-8's operational land imager (OLI) sensor was installed on the satellite on December 4, 2021. Software ArcGIS 10.8 and QGIS 3.8 were utilized to conduct the analysis. Maps for the land use land cover, land surface temperature (LST), Normalized Difference Vegetation Index (NDVI), and tasselled cap transformation (TCT) of the Old Oyo National Park were created as a result of the image analysis procedure. This study investigated how the tasselled cap transformation indices and land surface temperature are related to one another. Maps of the study area's NDVI, Tasseled Cap Transformation (TCT), and land surface temperature were produced using the image analysis procedure. The analysis indicates that the study area's land surface temperature (LST) ranges from 19.47 to 33.15 ^{o}C. It was discovered that the land surface temperature and the brightness index had a significant positive correlation (r = 0.95). Conversely, there was a relatively strong inverse relationship (r = -0.78) between LST and greenness index.

Keywords: Tasselled Cap Transformation, Greenness coefficient, Brightness coefficient, Wetness

Introduction

Various paths have demonstrated that changes in land use land cover (LULC) have a significant impact on the climate. These pathways are discovered to alter the surface energy balance, which then impacts the land surface temperature (LST), causing changes in the area's microclimate (Jain *et al*., 2017; Wang *et al*., 2018; Gogoi *et al*., 2019). LST remote sensing modelling provides a range of applications. The use of this technique in thermal environmental investigations has therefore increased quickly (Liu *et al*., 2018; Wang *et al*., 2018).

Remote sensing data and geographic information systems (GIS) are becoming more and more effective in extracting biophysical components, tracking dynamic changes in LULC, and mapping forest ecosystems (Bhagyanagar *et al*., 2012; Kimuku *et al*., 2017; Firozjaei *et al*., 2019). Numerous studies have been conducted on the relationship between Land Surface Temperature (LST) and LULC, and it has been found that one of the main consequences of LULC changes, particularly in metropolitan areas, is a rise in land surface

Journal of Forestry Research and Management. Vol. 19(4).18-30; 2022, ISSN 0189-8418
www.jfrm.org.ng

temperatures (LST) (Pal and Ziaul, 2017; Aboelnour and Engel, 2018).

This study is unique in the sense that it is focusing on LST variability in relations to tasselled cap transformation derivatives. This explains the importance of remote sensing and GIS as an apparent and preferred alternative when compared to the expensive and time-consuming conventional methods (Jeevalakshmi *et. al.,* 2017). The Normalized Difference Vegetation Index (NDVI), the LST, and the tasselled cap indices were examined using linear regression (Balcik and Ergene 2016; Guha *et al*., 2018; Ferrelli *et al*., 2018; Mohammad *et al.,* 2019). For instance, Mohammad *et al.,* (2019) in their study using the Tasselled cap indices, showed the regression results (LST-NDVI, R^2 = 0.65; LST-Brightness, R^2 = 0.65 and LST-Wetness, R^2 = 0.53) between LST and the Tasselled cap transformations. Therefore, phenological dynamics can be inferred from changes in vegetation and tasselled cap indices. A popular vegetation index that aids in understanding the relative biomass in a given area is the Normalized Difference Vegetation Index (NDVI). The single-band dataset that solely displays vegetation is provided as the derived output of the NDVI technique. The NDVI value ranges from -1 to +1. Rock and bare soil are represented by values closer to zero while vegetation is represented by values greater than +0.1. Vegetation becomes greener as the positive NDVI value rises. When compared to other sources of satellite imagery, Landsat satellite imagery has a strong archival advantage and offers lengthy time-series data for regional application studies (Muhammad *et al*., 2014).

The most important variable in determining a location's hottest and lowest temperatures is LST. Land cover or vegetation mapping at the regional and local scale is ideal for data with a medium spatial resolution, such as that from the LANDSAT. The Operational Land Imager (OLI) and the Thermal Infrared Sensor are the two instruments that LANDSAT 8 carries (TIRS). Eight bands in the visible, near-infrared, and shortwave infrared areas of the electromagnetic spectrum are used by OLI to collect data at a spatial resolution of 30m. An extra panchromatic band with a spatial resolution of 15m is also collected by OLI. Two bands located in the atmospheric window between 10 and 12 m are used by TIRS to detect the TIR radiance with a spatial precision of 100 m. (Anandababu *et al.*, 2018).

Researchers who had a spatial reference in meteorology typically use remote sensing data since they are fundamentally inexpensive and readily available (Karnieli *et al*., 2010). The shape that resulted from the graphical distribution of plotted data gave rise to the moniker "Tasselled Cap" (Kauth and Thomas, 1976). It creates composite values out of the readings from several channels. One of these weighted sums generally calculates the brightness of each pixel in the image, while another composite calculates the pixels' degree of greenness and another one may calculate the vegetation's degree of yellowness or the soil's degree of moisture (Kauth and Thomas, 1976). The purpose of this study is to investigate the correlation between land surface temperature and tasselled cap indicators.

Materials and Methods

Old Oyo National Park (OONP) is located between latitudes 8°10’ and 9°05´N and longitudes 3°35´ and 4°20´E (Figure 1). It has a total land mass of 261,345 ha, making it the fourth largest park in Nigeria (Mengistu and Salami, 2007). It is bordered in the North by Kwara State, in the South by Ikoyi while in

the western part is bordered by towns such as Igbope and Sepeteri. The adjoining communities are Igbeti, Balelayo, Oloka, Igboho, Abaja and Gboguro. The vegetation of the park has been classified as Southern Guinea Savanna. However, more studies classified the Southern portion of the vegetation as Forest savanna Mosaics with wooded savanna containing a relic of the moist semi-deciduous forest, grading northwards into drier mixed leguminous wooded Savanna with a continuous lower stratum of perennial grasses (Okosodo *et al*., 2016).

Topographically, it lies on a lowland between 330m and 508m above sea level, underpinned by the basement complex rocks. There are three watersheds in Old Oyo National Park: River Ogun and its numerous tributaries, River Tessi and its tributaries and River Iwa and its tributaries. Ogun River flows southwards to the Atlantic Ocean. Several tributaries notably Oopo, Iwawa, Oowe and Owu flow southwestwards and southeastwards to join it before its exit from the park. The Tessi River and Iwa River flow northwards to the River Niger. Three main tributaries including River Soro join it before it exits from the park. (Okosodo *et al*., 2016).

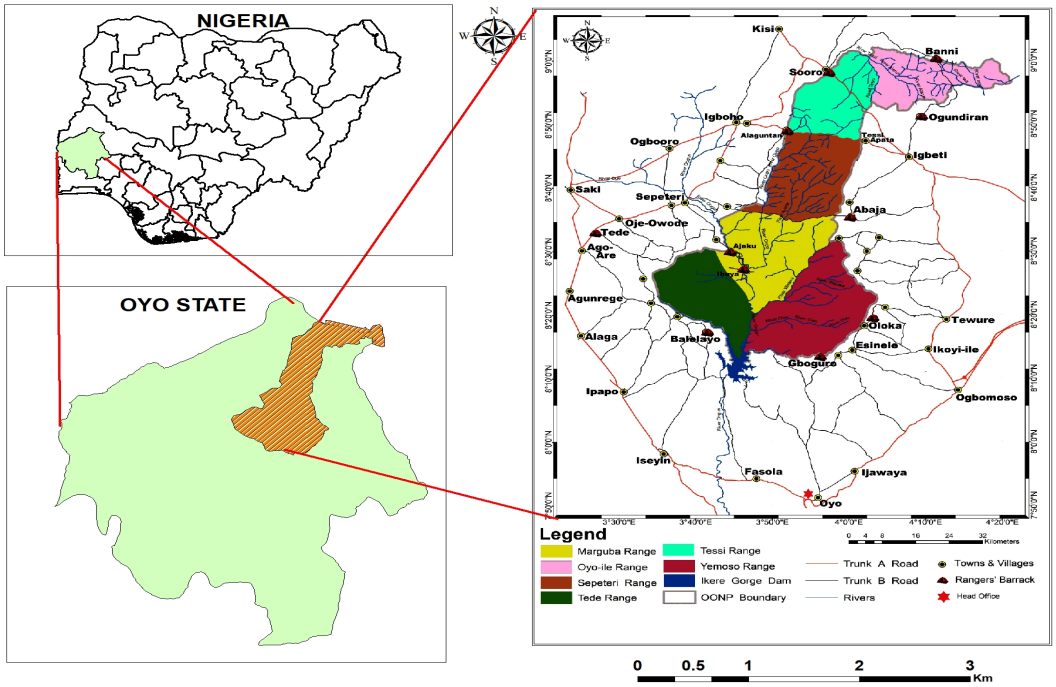

Figure 1: Location map of the study area (Old Oyo National Park)

The major data source for this research is Landsat 8 Operational Land Imager (OLI)/Thermal Infrared Sensor (TIRS) of December 4th 2021, which was obtained from the United States Geological Survey (USGS) website at https://earthexplorer.usgs.gov. The choice of the date is predicated on the need for a dry season data in order to minimize the effects of precipitation, and the availability of cloud-free Landsat data for flawless analysis. ArcGIS Spatial Analyst (version 10.8.2) and QGIS 3.16.3 were used for image processing.

Journal of Forestry Research and Management. Vol. 19(4).18-30; 2022, ISSN 0189-8418
www.jfrm.org.ng

Table 1 displays the attributes of the Landsat 8 image. Band 2 (blue), Band 3 (green), Band 4 (red), Band 5 (NIR), Band 6 (SWI and R1), and Band 7 (SWIR2) were used in the tasselled cap transformation equation to calculate the brightness, greenness, and wetness components

. **Table 1: Properties of Landsat 8 (OLI & TIRS) image**

Band	Name	Wavelength (micrometres)	Resolution
Band 1	Coastal aerosol	0.43 - 0.45	30
Band 2	Blue	0.45 - 0.51	30
Band 3	Green	0.53 - 0.59	30
Band 4	Red	0.64 - 0.67	30
Band 5	Near Infrared (NIR)	0.85 - 0.88	30
Band 6	SWIR 1	1.57 - 1.65	30
Band 7	SWIR 2	2.11 - 2.29	30
Band 8	Panchromatic	0.50 - 0.68	15
Band 9	Cirrus	1.36 - 1.38	30
Band 10	Thermal Infrared (TIRS) 1	10.60 - 11.19	100
Band 11	Thermal Infrared (TIRS) 2	11.50 - 12.51	100

Image Pre-processing

The Landsat 8 satellite image data that served as the research data had radiometric corrections applied during the pre-processing stage. To improve the accuracy of the information obtained from satellite image data, radiometric corrections are used to correct and eliminate surface reflection inaccuracies, sunlight direction, meteorological conditions, air disturbances, and other factors (Main *et al*., 2011). The analysis of multi-temporal and multi-sensory data for analyzing and spotting ongoing changes is another application of the correction (Kustiyo *et al.*, 2014). The satellite image was preprocessed by converting the image's metadata file's reflectance rescaling coefficients to Top of Atmosphere (TOA) planetary reflectance values. To transform Digital Numbers (DN) into TOA, utilize Equation 1.

$$\rho_\lambda = M_\rho \times Q_{cal} + A_\rho \quad (1)$$

Where,

ρλ= TOA planetary reflectance, without correction for solar angle.
Mρ= Band-specific multiplicative rescaling factor
Aρ = Band-specific additive rescaling factor
Q cal = pixel values (DN).

Correcting the Reflectance value with the Sun angle

Since the Sun angle at the moment of image acquisition was not taken into account, TOA reflectance values were not calibrated as a result. To adjust the reflectance values based on the angle of the Sun, the following equation was utilized.

$$\rho_{\lambda\,corrected} = {}^{\rho\lambda}/_{\sin\theta\,SE} \quad (2)$$

Where,
Pλ corrected = reflectance values after sun angle correction
ρλ = TOA planetary reflectance
θSE = Local sun elevation angle (sun angle).

Land-Use/Land-Cover Map Preparation

The procedure of classifying images was done using a supervised classification system. Using a Maximum Likelihood classifier, training sets were chosen for picture classification. To identify each class, 120 spectral signatures from the study image were gathered and combined. The land-use/land-cover types were divided into five classes using image classification, including thick forest, Light Forest, Shrubs, and Waterbody.

Land Surface Temperature (LST)

Conversion to at-satellite Brightness Temperature (Tb)

Before being converted to top-of-the-atmosphere (TOA) radiance, the digital numbers of the thermal band were calibrated to reduce the noise brought on by particles, water vapour, etc (Equation 3)

$$R = M_L \times Band\ 10_{DN} + A_L \quad (3)$$

Where,
R is TOA radiance (watts/ (meter squared * ster * μm),
ML and AL were also obtained from the header file of the Landsat 8 image.

Thereafter, the radiance (R) image of the Landsat sensor was converted to at-satellite brightness temperature (Equation 4).

$$T_b = \frac{K_2}{\ln(K_1/R)+1} \quad (4)$$

Where
T_b is at-satellite brightness temperature or black body temperature,
R is radiance while K_1 (watts/meter squared * ster * μm)
K_1 and K_2 (kelvin) are constants which are 774.89 and 1321.08 respectively.

In the image header file, the K1 and K2 constants for Landsat sensors are listed. Tb is not the actual surface temperature, as numerous authors have noted, because of air interference and differences in land cover (Hu and Jia, 2010). The noise in this investigation was eliminated using the single-channel atmospheric correction method developed by Sobrino *et al.,* 2004.

Determination of surface emissivity (ε)

Surface emissivity (**ε**) on ground surfaces varies with land coverings (Sun, 2017). In urban settings, vegetated surfaces outperform non-vegetated regions in terms of thermal holding capacity and cooling benefits. Now, the Proportion of Vegetation (Pv), which evaluates the significance of vegetation in each pixel of the satellite pictures, is estimated using the Normalized Difference Vegetation Index (NDVI) Equations 5 and 6 allow for the computation of these.

$$NDVI = \frac{NIR-RED}{NIR+RED} \quad (5)$$

$$P_v = \left[\frac{NDVI-NDVI_{min}}{NDVI_{max}-NDVI_{min}}\right]^2 \quad (6)$$

Where,

$NDVI_{min}$ and $NDVI_{max}$ were the maximum and minimum values obtained from the derived vegetation index image (Sobrino, 2008).

Using the formula developed by Sobrino *et al.,* (2004) in Equation 7, the relationships between and the proportion of vegetation (Pv) are measured on a variety of ground surfaces based on the extracted NDVI from Landsat.

$$\varepsilon = \begin{cases} 0.979 - 0.035Red & NDVI < NDVI_{min} \\ 0.986 + 0.004P_v & NDVI_{min} \le NDVI \le NDVI_{max} \\ 0.99 & NDVI > NDVI_{max} \end{cases} \quad (7)$$

Journal of Forestry Research and Management. Vol. 19(4).18-30; 2022, ISSN 0189-8418
www.jfrm.org.ng

Where
ε is the surface emissivity image and Red is the surface reflectance of the Red band.

Conversion of at-satellite brightness temperature to LST

Finally, the brightness temperature picture was transformed into Land Surface Temperature (LST) using the Planks equation as specified in Equation 8 using the predicted land surface emissivity for the Landsat 8 image (Weng *et al*., 2004)

$$LST_{KELVIN} = \frac{T_b}{1+(\lambda+T_b/\rho)*ln\ \varepsilon} \quad 8$$

Where
λ is the wavelength of radiation emitted in Landsat 8
ρ is h * c/σ,
σ is the Stefan Boltzmann's constant,
h is Plank's constant,
C is the velocity of light,
ε = surface emissivity image

Conversion of LST from Kelvin to Degrees Celsius

Using the relation of °C equals 273.15 K, the above-derived LSTs' unit was converted to degrees Celsius for ease of comprehension (Pal and Ziaul, 2016).

NDVI map derivation

Red and near-infrared (NIR) reflectance measurements were used to generate the Normalized Difference Vegetation Index (NDVI) (Liu and Zhang, 2011). Equation 9 uses Band 5 (for Landsat 8) and Band 4 to represent the NDVI (For Landsat 8).

$$NDVI = \frac{NIR-RED}{NIR+RED} \quad 9$$

Deriving Tasselled Cap Indices

The tasselled cap indices indicate each pixel's Greenness, Brightness, and Wetness. A linear combination of Landsat bands is used (From band 2 to band 7). The following equation was used to determine tasselled cap indices. Brightness is affected by the same physical factors that affect total reflectance. The attribute of healthy green vegetation—high chlorophyll absorption in the visible bands and high leaf structure reflectance in the near-infrared band responds to the colour green. The quantity of moisture that the soil or vegetation can hold affects the brightness, moisture, and greenery of the forest. Table 2 provides the required coefficient for use in transform equation 10 after components were determined using that equation.

$$Tas\_cap\ i = (coeff_2 * band2) + (coeff_3 * band3) + (coeff_4 * band4) + (coeff_5 * band5) + (coeff_6 * band6) + (coeff_7 * band7) \quad 10$$

Where,
Tas_cap i = Calculated tasselled cap index (Greenness, Brightness or Wetness)
Coeff = Corresponding co-efficient values for each band
Band = Preprocessed bands'

Table 2: Coefficient values of TCT for Landsat 8 (OLI) bands **(**Muhammad *et al*., 2014)

Components	Band-2 Blue	Band-3 Green	Band-4 Red	Band-5 NIR	Band-6 SWINR-1	Band-7 SWINR-2
Brightness	0.3037	0.2793	0.4743	0.5585	0.5082	0.1863
Greenness	-0.2848	-0.2435	-0.5436	0.7243	0.0840	-0.1800
Wetness	0.1509	0.1973	0.3279	0.3406	-0.7112	-0.4572

Journal of Forestry Research and Management. Vol. 19(4).18-30; 2022, ISSN 0189-8418
www.jfrm.org.ng

Regression Analysis

The System for Automated Geoscientific Analyses (SAGA) GIS software was used to calculate the regression equation between LST and NDVI, Brightness, Greenness, and Wetness. The three tasselled cap indices, along with all of the pixels of LST and NDVI, were used in the regression analysis because it has been shown that vegetative health has a significant impact on LST. LST remained the dependent variable while the NDVI and tasselled cap indices were considered independent factors (Zhang *et al*., 2010). In the vast majority of examinations, it has been discovered that the LST and NDVI do not correlate well.

Results and Discussion

Relationship between LULC class and LST

The Tessi Range and Sepeteri Range of the park include the majority of the thick forest class, according to the LULC map of the research area (Figure 2). In the other ranges, the light woodland and bushes predominate greatly. These LULC classes represent total area extents for the heavy forest, light forest, shrubs, and water body are 136633.05 ha, 114289.74 ha, 10091.79 ha, and 330.66 ha, respectively (Table 3). The same table displays the LST mean temperature values for each class. For dense woodland, light forest, bushes, and water bodies, they are 24.69°C, 23.99°C, 25.42°C, and 21.23°C, respectively.

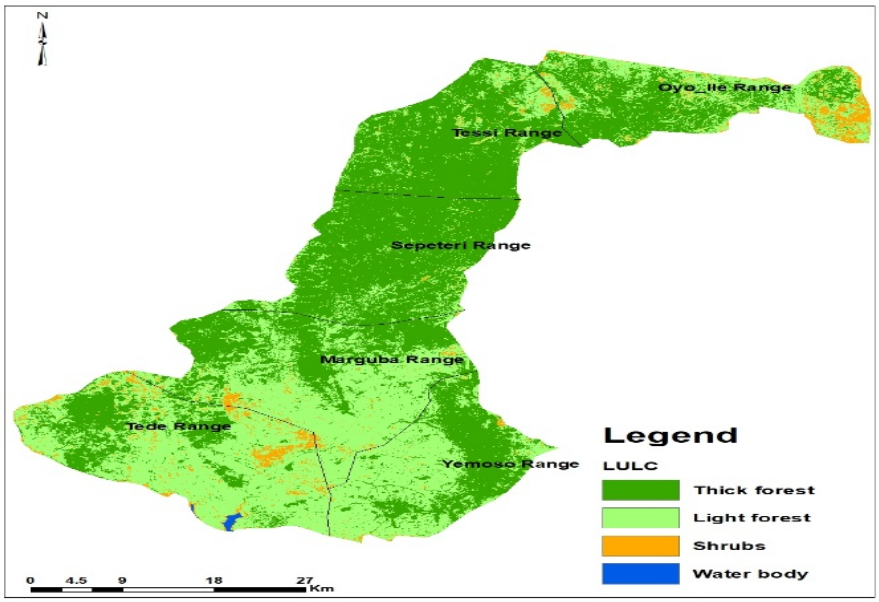

Figure 2: Land use land cover (LULC) of the study area

The shrubs LULC class has the highest temperature (25.42^{o}C). This can be attributed to the lack of dense canopy trees that could potentially moderate radiation. In the Oyo-ile Range and Tede Range, this class predominates greatly (Figure 2). The aquatic body registered the lowest temperature (21.23^{o}C). The LST distribution in the research area was further depicted in Figure 3. The analyses' findings concur with those of other studies that have examined the rise in

LST brought on by LULC changes (Pal and Ziaul 2016; Gogoi *et al*., 2019).

Table 3: Statistics of both LULC and the LST of the study area.

LULC Statistics			Corresponding Land Surface Temperature Derivatives			
LULC Class	Area (Ha)	Area (%)	MIM	MAX	MEAN	STD
Thick Forest	136633.05	52.28	19.51	29.82	24.69	1.48
Light Forest	114289.74	43.73	19.49	31.77	23.99	1.79
Shrubs	10091.79	3.86	20.23	33.15	25.42	2.64
Water Body	330.66	0.13	20.91	22.22	21.23	0.14

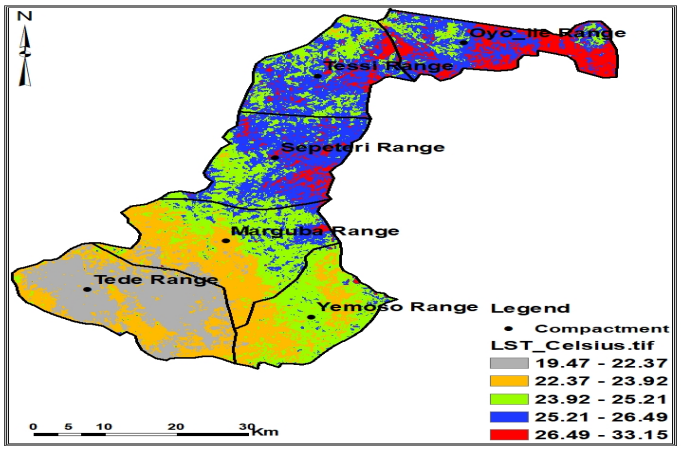

Figure 3. Geographical distribution of land surface temperature

The study area's Land Surface Temperature (LST) is between 19.47 and 33.15 ^{o}C. (Figure 3). Tede Range is where the lowest LSTs are found, with values less than 22.37 ^{o}C. Oyo-ile Range, Tessi Range and Sepeteri Range had the highest temperatures (26.49 to 33.15^{o}C).

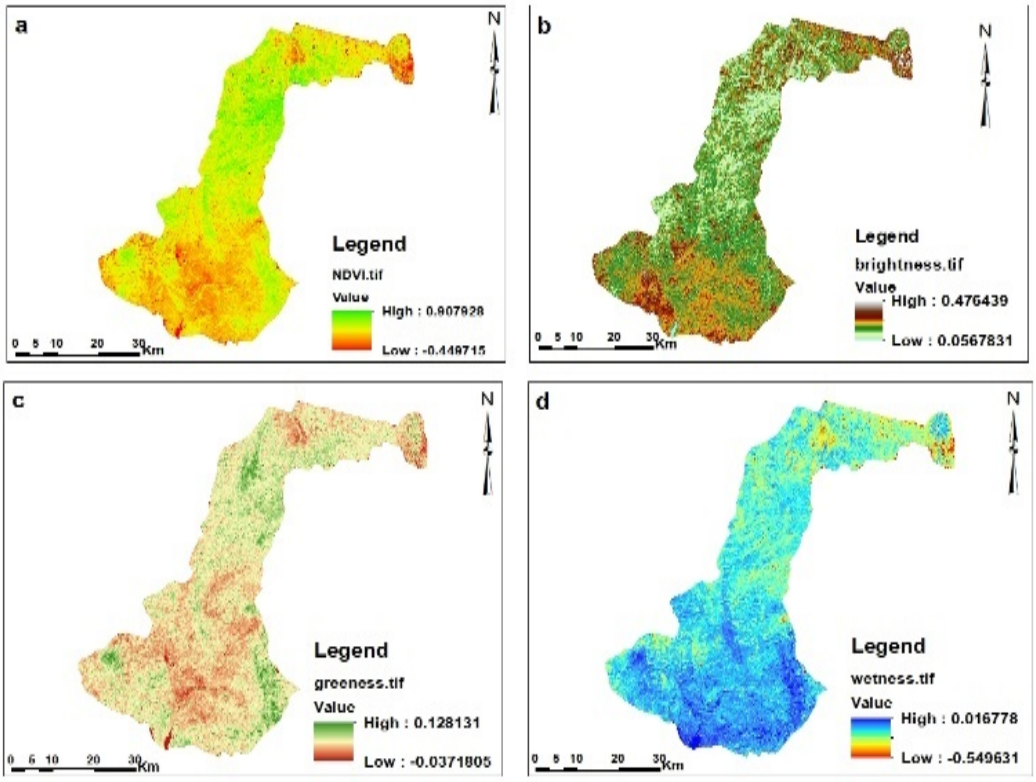

Figure 4: Maps of (a) NDVI (b) Brightness (c) Greenness and (d) Wetness of the study area.

Relationship between LST and NDVI, Brightness, Greenness and Wetness.

The values of the NDVI range from -0.45 to 0.91. (Figure 4). The Tessi Range and Sepetari Range axis of the research region includes the majority of the highest NDVI values. It supports the classification by demonstrating how heavily represented the thematic classes of thick and light forests are in these two ranges.

Journal of Forestry Research and Management. Vol. 19(4).18-30; 2022, ISSN 0189-8418
www.jfrm.org.ng

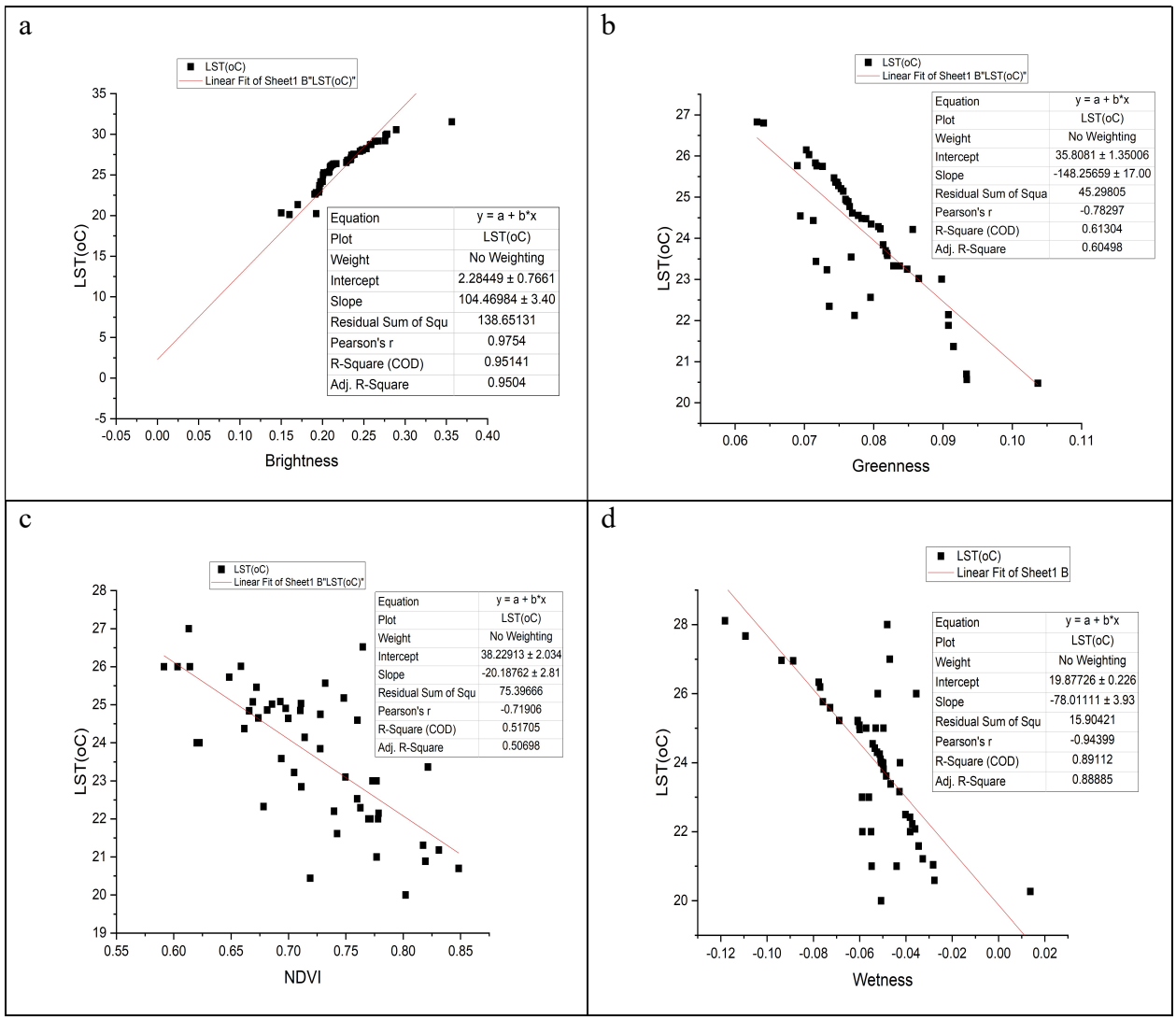

Figure 5: The results of regression analysis between LST and (a) Brightness (b) Greenness (c) NDVI (d) Wetness at the Old Oyo National Park (OONP)

Figure 5a shows a significant positive connection (r = 0.95) between surface temperature and brightness index. The study area's upper and middle portions experience some of the greatest temperatures, in part due to the highest brightness index values. Brightness among the tasselled cap indices takes into account topographic changes, bare or partially covered soil, and natural and road characteristics (Eva *et al.*, 2007). The relationship between surface temperature and the greenness index is quite inverse (r = -0.78; Figure 5b). However, generally speaking, places with a lot of greenery will have cooler surface temperatures.

The Normalized Difference Vegetation Index, gauges the density and vitality of vegetation at the surface. It was determined through correlation analysis that there was a high negative relationship (r = -0.78; Figure 5b) between LST and NDVI. The substantial negative correlation of NDVI with LST

implies that good green vegetation decreases surface temperature. The spatial distribution of surface temperature in the study area and the wetness factor, which measures the quantity of soil moisture, agree well. There is a very high inverse correlation between LST and wetness index (Figure 5d, r = -0.94). This implies that the LST will drop as the wetness index rises. For instance, the LST in the southern region of the research area (Tede Range) with a predominance of wetness ranges from 19.47 to 22.37 ^{o}C. (Figure 3).

Conclusion

The Old Oyo National Park's LST relationship, tasselled cap indices, and NDVI study revealed that temperatures there vary from 19 to 33 °C. Due to the inverse link between LST and NDVI, heavy vegetation conditions can alter the forest's thermal properties. Because high vegetation absorbs heat energy emitted by surface features, surface temperatures are recorded at lower levels. While tasselled cap indices offer more spectral details regarding the land use and land cover of the research area, an in-depth description of vegetation health and land cover was further explained using NDVI maps. However, the greenness index can offer far more proof to support the assessment of the state of the vegetation in a specific area established using NDVI measurement

REFERENCES

Aboelnour M, Engel BA (2018). Application of remote sensing techniques and geographic information systems to analyze land surface temperature in response to land use/land cover change in Greater Cairo Region, *Egypt. Journal of Geographic Information System* 10(01), 57.

Anandababu, B M Purushothaman, Babu S. Suresh (2018). Estimation of and Surface Temperature using LANDSAT 8 Data. *International Journal of Advance Research, Ideas and Innovations in Technology,* 4 (2), 177-186.

Balcik F. B., Ergene E. M. (2016). Determining The Impacts of Land Cover/Use Categories on Land Surface Temperature using Landsat 8 - OLI. The International Archives of the Photogrammetry, Remote Sensing and Spatial Information Sciences, Volume XLI-B8, 2016 XXIII ISPRS Congress, 12–19 July 2016, Prague, Czech Republic.

Bhagyanagar, R., Kawal, B.M., Dwarakish, G.S. and Surathkal, S. (2012) Land Use/Land Cover Change and Urban Expansion during 1983-2008 in the Coastal Area of Dakshina Kannada District, South India. *Journal of Applied Remote Sensing,* 6,63576.https://doi.org/10.1117/1.JRS.6.063576

Eva, lvits, Alistair, L., Filip, L., Scott, H. and Barbara, K.(2008). Orthogonal Transformation of Segmented SPOT5 Images: Seasonal and Geographical Dependence of the Tasselled Cap Parameters, *Photogrammetric Engineering and Remote Sensing,* 74(11), 1351-1364.

Ferrelli, F., Huamantinco Cisneros, M. A., Delgado, A. L., & Piccolo, M. C. (2018). Spatial and temporal analysis of the LST-NDVI relationship for the study of land cover changes and their contribution to urban planning in Monte Hermoso, Argentina.*Documents d'AnàlisaGeogràphica,* 64(1), 25-47.

Firozjaei, M. K., Alavipanah, S. K., Liu, H., Sedighi, A., Mijani, N., Kiavarz, M., & Weng, Q. (2019). A PCA–OLS Model for Assessing the Impact of Surface Biophysical Parameters on Land Surface Temperature Variations. *Remote Sensing,* 11(18), 2094.

Gogoi, P. P., Vinoj, V., Swain, D., Roberts, G., Dash, J., and Tripathy, S. (2019). Land use and land cover change effect on surface temperature over Eastern India. Scientific reports, 9(1), 1- 10.

Guha, S., Govil, H., Dey, A., and Gill, N. (2018). Analytical study of land surface temperature with NDVI and NDBI using Landsat 8 OLI and TIRS data in Florence and Naples city, Italy. *European Journal of Remote Sensing,* 51(1), 667-678.

Hu, Y. and Jia, G. (2010) Influence of land use change on urban heat island derived from multi-sensor data. International *Journal of Climatology*, 30(9),1382–1395. doi: 10.1002/joc.1984

Jain, M., Dimri, A. P., & Niyogi, D. (2017). Land-Air Interactions over Urban-Rural Transects Using Satellite Observations: Analysis over Delhi, India from 1991–2016. *Remote Sensing,* 9(12), 1283.

Jeevalakshmi, D & Narayana Reddy, S & Manikiam, Balakrishnan. (2017). Land surface temperature retrieval from LANDSAT data using emissivity estimation. *International Journal of Applied Engineering Research.* 12. 9679-9687.

Karnieli A, Agam N, Pinker RT, Anderson M, Imhoff ML, Gutman GG (2010). Use of NDVI and land surface temperature for drought assessment: Merits and limitations. Journal of Climate 23, 618-633. http://dx.doi.org/10.1175/2009JCLI2900.1

Kauth R.J. and Thomas G.S. (**1976)**. The Tasselled Cap –A Graphic Description of the Spectraltemporal development of agricultural crops as seen in Landsat, in Proceedings of the Symposium on Machine Processing of Remotely Sensed Data, University, West Lafayette, Indiana.

Kimuku, C.W. and Ngigi, M. (2017). Study of Urban Heat Island Trends to Aid in Urban Planning in Nakuru County-Kenya. *Journal of Geographic Information System,* 9, 309-325.

Kustiyo, Dewanti R, and Lolitasari, I.: (DATE?) PengembanganMetodaKoreksiRadiometrik Citra SPOT 4 Multi－Spektral dan Multi－Temporal UntukMosaik Citra. Pusat Teknologi dan Data PenginderaanJauh, LAPAN, Indonesia, (2014).

Liu Y, Song W, Deng X (2018). Understanding the spatiotemporal variation of urban land expansion in oasis cities by integrating remote sensing and multi-dimensional DPSIR-based indicators. *Ecological Indicators,* 96,23-37.

Liu, L. and Zhang, Y. (2011). Urban heat island analysis using the Landsat TM data and ASTER Data: A case study in Hong Kong", Remote Sensing, 3(7),1535–1552. doi: 10.3390/rs3071535

Main, R., Cho, M.A., Mathieu, R., O'Kennedy, M.M., Ramoelo, A., and Koch, S. (2011). An Investigation into Robust Spectral Indices for Leaf Chlorophyll Estimation. *ISPRS Journal of Photogrammetry and Remote Sensing,* 66, 751－761.

Mengistu, and Salami (2007). Application of remote sensing and GIS in land use/land cover mapping and change detection in a part of southwestern Nigeria. *African. J. Environ. Sci. Technology.*1(5),099 -109

Muhammad Hasan Ali Baig, Lifu Zhang, Tong Shuai, and Qingxi Tong(2014).Derivation of a tasselled cap transformation based on Landsat 8 at-satellite reflectance, *Remote Sensing Letters,* 5(5),423-431.

Mohammad Subzar Malik, Jai Prakash Shukla and Satanand Mishra (2019). Relationship of LST, NDBI and NDVI using Landsat-8 data in Kandaihimmat Watershed, Hoshangabad, India. *Indian Journal of Geo*

Marine Sciences. 48 (01), January 2019, 25-31

Okosodo E. F., Orimaye J. O., Awoyemi A. G. (2016). Diversity and Abundance of Avian Species in Old Oyo National Park Southwest Nigeria. *Merit Research Journal of Agricultural Science and Soil Sciences* 4(11) 147-157

Pal, S. and Ziaul, S. (2016). Detection of land use and land cover change and land surface temperature in English Bazar urban centre, *The Egyptian Journal of Remote Sensing and Space Sciences.* National Authority for Remote Sensing and Space Sciences. doi: 10.1016/j.ejrs.

Pal, S. and Ziaul, S. K. (2017). Detection of land use and land cover change and land surface temperature in English Bazar urban centre. *The Egyptian Journal of Remote Sensing and Space Science,* 20(1), 125-145.

Sobrino, J. A.(2008). Land surface emissivity retrieval from different VNIR and TIR sensors, IEEE Transactions on Geoscience and Remote Sensing, 46(2), 316–327. doi: 10.1109/TGRS.2007.904834.

Sobrino, J. A., Jiménez-Muñoz, J. C. and Paolini, L. (2004) Land surface temperature retrieval from LANDSAT TM 5, *Remote Sensing of Environment,* 90(4), 434–440.

Sun, Z. (2017). A modified normalized difference impervious surface index (MNDISI) for automatic urban mapping from Landsat imagery, *Remote Sensing,* 9(9). doi: 10.3390/rs9090942.

Wang, Y. C., Hu, B. K., Myint, S. W., Feng, C. C., Chow, W. T., & Passy, P. F. (2018). Patterns of land change and their potential impacts on land surface temperature change in Yangon, Myanmar. *Science of the Total Environment,* 643, 738-750.

Weng, Q., Lu, D., and Schubring, J. (2004). Estimation of land surface temperature–vegetation abundance relationship for urban heat island studies. *Remote sensing of Environment*, 89(4), 467-483.

Zhang, X.X., Wu, P.F., Chen, B. (2020). Relationship between vegetation greenness and urban heat island effect in Beijing City of China. *Procedia Environ. Sci.* 2, 1438–1450.